Localization of $^{23}Na^+$ in a DNA Quadruplex by High-Field Solid-State NMR

David Rovnyak,[†] Marc Baldus,[†] Gang Wu,[‡] Nicholas V. Hud,[§,⊥] Juli Feigon,[§] and Robert G. Griffin*[,§]

Contribution from the MIT/Harvard Center for Magnetic Resonance, Francis Bitter Magnet Laboratory and Department of Chemistry, Massachusetts Institute of Technology, 77 Massachusetts Avenue, Cambridge, Massachusetts 02139, Department of Chemistry, Queen's University, Kingston, Ontario K7L 3N6, Canada, and Department of Chemistry and Biochemistry and the Molecular Biology Institute, University of California, Los Angeles, 405 Hilgard Avenue, Los Angeles, California 90095-1569

Received March 22, 2000. Revised Manuscript Received August 28, 2000

Abstract: Monovalent cations such as Na^+, K^+, and NH_4^+ are known to stabilize DNA quadruplexes formed of guanine-quartets. Such structures readily form from the guanine-rich repeat sequences found in telomeres, the physical ends of eukaryotic chromosomes. We present a solid-state NMR approach for studying ions associated with G-quartets based on the direct NMR observation of $^{23}Na^+$ ion resonances and report new methods for studying quadrupolar nuclei in biological solids. In the tetraplex forming oligonucleotide d(TG_4T), high-field (17.6 T) NMR spectra cleanly resolve three distinct classes of sodium ions. A high-resolution 2D-MQMAS spectrum established the assignment of an amorphously broadened signal at −19 ppm (relative to 0.1 M NaCl) to surface-bound Na^+ ions. Two-dimensional nutation spectroscopy was used to indicate the relative size of the quadrupole coupling for each line, while a standard exchange experiment established a correlation between surface (−19 ppm) and channel-bound (6.8 ppm) Na^+ ions. Finally, free sodium ions are observed at 0 ppm. This work demonstrates the utility of high field spectroscopy in combination with a suite of 2D solid-state NMR experiments for resolving and assigning multiple Na^+ sites in $[d(TG_4T)]_4$.

I. Introduction

DNA oligonucleotides containing one or more appropriately spaced runs of guanines can associate to form intra- or intermolecular quadruplexes composed of stacked hydrogen bonded guanine quartets (Figure 1a).[1] The G-quartets are stabilized by coordination of the guanine carbonyls to specific monovalent (e.g., Na^+, K^+, NH_4^+) or divalent (e.g., Sr^{2+}) cations which bind either in the plane of the quartet or between pairs of quartets. Cation-stabilized, guanine quadruplexes have been shown to readily form from the guanine-rich repeat sequences found in telomeres, the terminal sequences of eukaryotic chromosomes, imparting stability and resistance to chemical modification.[2−6] The length of the telomeric region shortens incrementally upon normal cell division and the cumulative loss of telomeric DNA eventually becomes lethal to somatic cells after a certain number of divisions.[7−11] Telomeric DNA consists of sequence repeats, where TTAGGG is the telomeric repeat in vertebrate somatic cells (T = thymine, A = adenosine). The DNA polymerase telomerase is capable of rebuilding the ends of telomeres by replacing these sequences on the telomere and has been shown to be active in 85−90% of human cancers and inactive in healthy, somatic cells.[12,13] Thus, there has been tremendous interest in determining the relationship between cell immortalization in cancer cells with the maintenance of telomere length. A significant finding is that stabilizing the G-quartet structure inhibits the activity of telomerase.[14−16] Recent progress in understanding the stabilization of guanine quartets includes the direct observation of coordinated cations in the solution state[17,18] and the development of small molecules which bind to tetraplex-forming DNA oligonucleotides.[15,19−22]

[†] Massachusetts Institute of Technology.
[‡] Queen's University.
[§] University of California, Los Angeles.
[⊥] Current address: School of Chemistry and Biochemistry, Georgia Institute of Technology, Atlanta, GA 30332-0400.

(1) Blackburn, E. H. *Nature* **1991**, *350*, 569−573.
(2) Guschlbauer, W.; Chantot, J.-F.; Thiele, D. J. *J. Biomol. Struct. Dyn.* **1990**, *8*, 491−511.
(3) Kang, C.; Zhang, X.; Ratliff, R.; Moyzis, R.; Rich, A. *Nature* **1992**, *356*, 126−131.
(4) Smith, F. W.; Feigon, J. *Nature* **1992**, *356*, 164−168.
(5) Williamson, J. R.; Raghuraman, M. K.; Cech, T. R. *Cell* **1989**, *59*, 871−880.
(6) Williamson, J. R. *Annu. Rev. Biophys. Biomol. Struct.* **1994**, *23*, 703−730.
(7) Wright, W. E.; Shay, J. W. *Trends Genet.* **1992**, *8*, 193−197.
(8) Hastie, N. D.; Dempster, M.; Dunlop, M. G.; Thompson, A. M.; Green, D. K.; Allshire, R. C. *Nature* **1990**, *346*, 866−868.
(9) Lindsey, J.; McGill, N. I.; Lindsey, L. A.; Green, D. K.; Cooke, H. J. *Mut. Res.* **1991**, *256*, 45−48.
(10) Allsopp, R. C.; Vaziri, H.; Patterson, C.; Goldstein, S.; Younglai, E. V.; Futcher, A. B.; Greider, C. W.; Harley, C. B. *Proc. Natl. Acad. Sci. U.S.A.* **1992**, *89*, 10114−10118.
(11) Vaziri, H.; Schachter, F.; Uchida, I.; Wei, L.; Zhu, X.; Effros, R.; Cohen, D.; Harley, C. B. *Am. J. Hum. Genet.* **1993**, *52*, 661−667.
(12) Hiyama, E.; Hiyama, K.; Yokoyama, T.; Matsuura, Y.; Piatyszek, M. A.; Shay, J. W. *Nature Med.* **1995**, *1*, 249−255.
(13) Kim, N. W.; Piatyszek, M. A.; Prowse, K. R.; Harley, C. B.; West, M. D.; Ho, P. L. C.; Coviello, G. M.; Wright, W. E.; Weinrich, S. L.; Shay, J. W. *Science* **1994**, *266*, 2011−2015.
(14) De Lange, T. *Proc. Natl. Acad. Sci. U.S.A.* **1994**, *91*, 2882−2885.
(15) Sun, S.; Thompson, B.; Cathers, B. E.; Salazar, M.; Kerwin, S. W.; Trent, J. O.; Jenkins, T. C.; Neidle, S.; Hurley, L. H. *J. Med. Chem.* **1997**, *40*, 2113−2116.
(16) Zahler, A. M.; Williamson, J. R.; Cech, T. R.; Prescott, D. M. *Nature* **1991**, *350*, 718−729.
(17) Hud, N. V.; Smith, F. W.; Anet, F. A. L.; Feigon, J. *Biochemistry* **1996**, *35*, 15383−15390.
(18) Hud, N. V.; Schultze, P.; Feigon, J. *J. Am. Chem. Soc.* **1998**, *120*, 6403−6404.

10.1021/ja001022o CCC: $19.00
Published on Web 11/03/2000

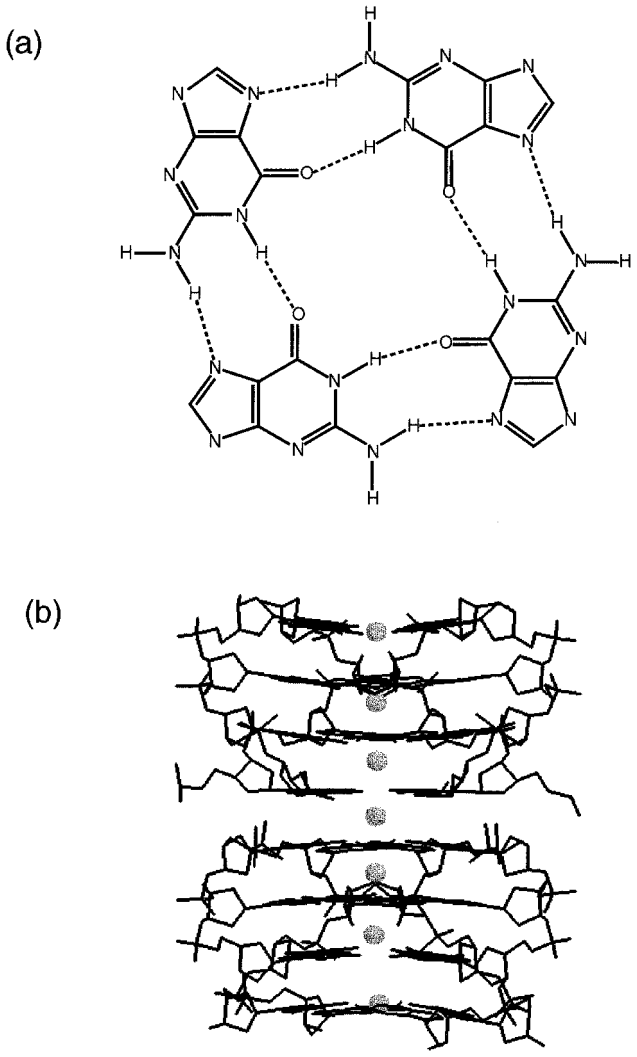

Figure 1. (a) Diagram illustrating the cyclic hydrogen bonding in a G-quartet. The monovalent cation, which can reside in or out of the guanine plane, is omitted in this representation. (b) Structure of the quadruplex formed by d(TG_4T), which shows the stacking of two $[d(TG_4T)]_4$ units to form an extended quadruplex with 8 G-quartets with the 7 Na^+ ions identified in the crystal structure [PDB:244d][42].

Recently, solution state NMR was employed by Hud et al., after substituting the ammonium ion, NH_4^+, in place of Na^+, to probe the cation binding sites in $[d(G_4T_4G_4)]_2$, which contains the repeat sequence d(T_4G_4) found in *Oxytricha nova* telomeres.[18] ^{1}H NMR established the existence and location of three monovalent cation sites in $[d(G_4T_4G_4)]_2$. While solution NMR is an established and mature tool for studying spin-$^1/_2$ nuclei in biological systems,[23−25] spectra of quadrupolar nuclei such as ^{23}Na and ^{39}K usually give rise to only a single resonance in solution NMR experiments and therefore it is difficult to draw conclusions about specific ion binding sites. However, quadrupolar nuclei are often located in the most significant regions of biomolecules[26,27] and can act as effective site-specific spin labels for NMR based studies. Solid-state NMR allows for the direct observation of half-integer quadrupoles in biomolecules and may provide access to these molecular regions and to the measurement of the quadrupole coupling constant, which is a sensitive reporter of local geometry (e.g., see refs 28 and 29).

In solid samples, longitudinal relaxation times of quadrupolar nuclei are long, but the spectral broadening due to the quadrupole coupling can limit the sensitivity and resolution of solid-state NMR spectra. The feasibility of observing nuclei such as ^{23}Na ($S = {}^3/_2$), ^{67}Zn ($S = {}^5/_2$), ^{17}O ($S = {}^5/_2$), and ^{59}Co ($S = {}^7/_2$) has been demonstrated by several authors,[30−38] where much of this progress has benefited from the recent development of the multiple-quantum magic-angle spinning (MQMAS)[39,40] experiment for recovering isotropic signals from quadrupolar nuclei in solids. Also, advances in instrumentation provide higher external fields which are critical for truncating the high-order quadrupolar coupling that is not averaged by magic-angle spinning (MAS). To date, however, there have been no demonstrations of $S > 1$ quadrupolar solid-state NMR in large biological macromolecules. We present a solid-state ^{23}Na NMR study in the tetraplex forming oligonucleotide d(TG_4T). In the crystal structure of this molecule,[41,42] four strands associate to form a stack of four guanine quartets, and two of these tetraplexes are stacked along their long axes to form a continuous helix of eight G-quartets with the end thymines looped out. A total of seven sodium ions are localized along the center of the two stacked quadruplexes (referred to hereafter as channel ions, see Figure 1b). Here we have used solid-state ^{23}Na NMR to study cation binding to this quadruplex. We use a new method for studying sample motions and a novel approach for making assignments, both of which exploit effects due to the quadrupolar coupling. By combining a number of high-field 2D experiments we directly observe three classes of Na^+ ions, corresponding to channel, surface, and free ions, with chemical shifts of 6.8, −19, and 0 ppm, respectively, relative to 0.1 M NaCl solution.

(19) Han, F. X.; Wheelhouse, R. T.; Hurley, L. H. *J. Am. Chem. Soc.* **1999**, *121*, 3561−3570.
(20) Perry, P. J.; Gowan, S. M.; Reszka, A. P.; Polucci, P.; Jenkins, T. C.; Kelland, L. R.; Neidle, S. *J. Med. Chem.* **1998**, *41*, 3253−3260.
(21) Anantha, N. V.; Azam, M.; Sheardy, R. D. *Biochemistry* **1998**, *37*, *7* (9), 2709−2714.
(22) Fedoroff, O. Y.; Salazar, M.; Han, H.; Chemeris, V. V.; Kerwin, S. M.; Hurley, L. H. *Biochemistry* **1998**, *37*, *7* (36), 12367−12374.
(23) Wuthrich, K. *NMR of Proteins and Nucleic Acids*; New York: Wiley-Interscience; 1986.
(24) Ernst, R. R.; Bodenhausen, G.; Wokaun, A. *Principles of Nuclear Magnetic Resonance in One and Two Dimensions*; Oxford: Clarendon Press, 1987.
(25) Cavanagh, J.; Fairbrother, W. J.; Palmer, A. G.; Skelton, N. J. *Protein NMR Spectroscopy: Principles and Practice*; San Diego, California: Academic Press: 1996.
(26) Saenger, W. *Principles of Nucleic Acid Structure*; *Springer Advanced Texts in Chemistry*; Cantor, C. R., Ed.; Springer-Verlag: New York, 1984.
(27) Lippard, S. J.; Berg, J. M. *Principles of Bioinorganic Chemistry*; University Science Book; Mill Valley, CA, 1994.
(28) Kentgens, A. P. M. *Geoderma* **1997**, *80*, 271−306.
(29) Baldus, M.; Meier, B. H.; Ernst, R. R.; Kentgens, A. P. M.; Meyer zu Altenschildesche, H. *J. Am. Chem. Soc.* **1995**, *117*, 5141−5147.
(30) Wu, G.; Rovnyak, D.; Huang, P. C.; Griffin, R. G. *Chem. Phys. Lett.* **1997**, *277*, 79−83.
(31) Medek, A.; Frydman, V.; Frydman, L. *J. Phys. Chem. B* **1997**, *101* (44), 8959−8966.
(32) Wu, G. *Chem. Phys. Lett.* **1998**, *298*, 375−380.
(33) Kunwar, A. C.; Turner, G. L.; Oldfield, E. *J. Magn. Reson.* **1986**, *69*, 124−127.
(34) Wu, G.; Rovnyak, D.; Griffin, R. G. *J. Am. Chem. Soc.* **1996**, *118*, *8* (39), 9326−9332.
(35) Medek, A.; Harwood: J. S.; Frydman, L. *J. Am. Chem. Soc.* **1995**, *117* (51), 12779−12787.
(36) Vosegaard, T.; Andersen, U.; Jakobsen, H. J. *J. Am. Chem. Soc.* **1999**, *121*, 1970−1971.
(37) Sham, S.; Wu, G. *Can. J. Chem.* **1999**, *77*, 1782.
(38) Larsen, F.; Lipton, A. S.; Jakobsen, H. J.; Nielsen, N. C.; Ellis, P. D. *J. Am. Chem. Soc.* **1999**, *121*, 3783−3784.
(39) Frydman, L.; Harwood: J. S. *J. Am. Chem. Soc.* **1995**, *117*, 5367−5368.
(40) Wu, G.; Rovnyak, D.; Sun, B.; Griffin, R. G. *Chem. Phys. Lett.* **1996**, *249*, 210−217.
(41) Phillips, K.; Dauter, Z.; Murchie, A. I. H.; Lilley, D. M. J.; Luisi, B. *J. Mol. Biol.* **1997**, 171−182.
(42) Laughlan, G.; Murchie, A. I. H.; Norman, D. G.; Moore, M. H.; Moody, P. C. E.; Lilley, D. M. J.; Luisi, B. *Science* **1994**, *265*, 520−524.

II. Background

i. Sensitivity of Quadrupolar NMR. The Hamiltonian for a quadrupolar nucleus must include terms for the Zeeman interaction and the coupling of the nuclear quadrupole moment with the surrounding electric field gradient. The dipolar coupling and chemical shift anisotropy can frequently be neglected as they are at least 1 or 2 orders of magnitude smaller than the Zeeman and quadrupolar interactions. The quadrupole coupling is typically evaluated to first and second orders in perturbation[43] and average-Hamiltonian[44,45] theories. The first-order frequency, which is usually several MHz, is quadratic in I_z and does not affect any symmetric transition, $(n/2, -n/2)$ but renders the side transitions, $(n/2, (n-1)/2)$, unobservable. The second-order term is linear in I_z and thus affects all transitions, introducing broadening in the kilohertz regime to the observable central transition (1/2, −1/2). This analysis requires $\omega_z > e^2qQ/h$, where ω_z is the Zeeman frequency and e^2qQ/h is the principal component of the quadrupole coupling tensor.

Although magic-angle spinning (MAS) leads to solution-like isotropic spectra of spin-$^1/_2$ nuclei in solids, MAS does not completely remove the anisotropy of the second-order quadrupolar term. Instead, when the sample is rotated about the magic angle, $\theta_m = 54.74°$, a residual line width Δ is observed, which can be estimated by the proportionality

$$\Delta \propto \omega_Q^2/\omega_0 \tag{1}$$

where ω_0 is the Larmor frequency of the quadrupolar nucleus (e.g., $\omega_0(^{23}Na)/2\pi = 198$ MHz at 17.6 T) and $\omega_Q = e^2qQ/h/2S(2S-1)$. Typical values of the quadrupole coupling are $e^2qQ/h \in [0,10]$ MHz, and the MAS line widths of half-integer quadrupolar nuclei such as ^{23}Na ($S = ^3/_2$) and ^{17}O ($S = ^5/_2$) are generally observed in the 1−30 kHz range in a 9.4-T static field (400 MHz for ^{1}H), severely compromising sensitivity and resolution. In eq 1 the inverse dependence of the line width on the static field results from incomplete truncation of the quadrupole coupling by the Zeeman interaction. To see how this affects the sensitivity of quadrupolar NMR, we first consider a system of identical spin-$^1/_2$ nuclei, for which the sensitivity difference of Fourier NMR spectroscopy at two static fields is approximately[46]

$$\Delta S = (B_0^f/B_0^i)^{3/2} \tag{2}$$

For simplicity we overlook some details in this comparison and the reader is referred to the monograph of Ernst et al.[24] and to Hoult and Richards[46] for further discussion on the sensitivity of FT-NMR. We see from eq 1 that doubling the static field halves the line width, thereby increasing the signal-to-noise ratio per scan by a factor of 2. Then eq 2 for a system of half-integer quadrupolar nuclei becomes

$$\Delta S' = (B_0^f/B_0^i)^{5/2} \tag{3}$$

In the case of $B_0^f = 17.6$ T versus $B_0^i = 9.4$ T, narrowing of the MAS line by a factor of ∼2 and an overall enhancement of 4.8 can be realized.

ii. Nutation of the Central-Transition and Triple-Quantum Subspaces. In spin-$^1/_2$ systems, nutation experiments are often employed to determine the homogeneity of the applied radio frequency field over the sample volume. These 2D experiments are composed of a single incrementable pulse, where a Fourier transform in the indirect dimension corresponds to a frequency histogram of the response of the spin system to continuous rf irradiation. If an rf field applied to a system of spin-$^1/_2$ nuclei corresponds to $\omega_1/2\pi = 50$ kHz, then the single-quantum coherence evolves with a period of 20 μs during the rf irradiation, corresponding to a 5-μs "90°" pulse length. In half-integer quadrupolar nuclei, the nutation behavior is not so simple and separate subspaces and limiting conditions must be considered. In doing so, we arrive at two experiments based on simple nutation concepts which can provide valuable insight into the spectroscopy of d(TG$_4$T).

Straightforward application of fictitious spin-$^1/_2$ operators leads to the following two nutation regimes for the central-transition (CT) of half-integer quadrupolar nuclei[47,48]

$$\omega_{1,eff}^{CT} = (S+1/2)\omega_1, \quad \omega_Q > \omega_1$$
$$\omega_{1,eff}^{CT} = \omega_1, \quad \omega_Q < \omega_1 \tag{4}$$

where ω_Q is the quadrupole coupling frequency, $\omega_Q = (e^2qQ/h)/[2S(2S-1)]$, and ω_1 is the strength of the applied rf field. In the regime of vanishing quadrupole coupling, the nutation behavior of the central-transition is identical to that for a spin-$^1/_2$. However, when the quadrupole coupling is large and $S = ^3/_2$, the *effective rf field* experienced by the central transition is twice the strength of the actual applied field. Hence a 50-kHz applied field would correspond to $\omega_{eff}^{CT}/2\pi$ kHz, requiring a 2.5-μs pulse length for a "selective 90°" pulse on the central transition. For half-integer quadrupolar nuclei, a 2D nutation experiment should distinguish between sites with vanishing and measurable quadrupole coupling frequencies since Fourier transformation along $\omega_1/2\pi$ will report ω_1 or $(S+1/2)\omega_1$ for each signal in the 1D MAS spectrum.

Similarly, fictitious spin-$^1/_2$ operators have been used in the triple quantum subspace for a $S = ^3/_2$ nucleus.[47,48] In the limit of a large quadrupole coupling constant, i.e., $\omega_Q \gg \omega_1$, the nutation frequency is $\omega_{1,eff}^{3Q} \propto (\omega_1^3/\omega_Q^2)$. However, the limit of a vanishing quadrupole coupling has received less attention. To predict the nutation of the triple quantum coherence in this regime, it is important to note that the first-order quadrupole term provides the coupling element which connects the central-transition and triple-quantum subspaces. Thus, when the quadrupole coupling is small compared to the applied rf field, increasing the quadrupole frequency should *increase* the 3Q nutation frequency. We tested this qualitative prediction with full numerical simulations of the 3Q nutation efficiency as a function of the quadrupole coupling in the regime $\omega_1 \gg \omega_Q$. The results are shown in Figure 2, where a fixed length nutation pulse results in increased 3Q coherence with increasing ω_Q up to the limit $\omega_Q \approx \omega_1$. We see in Figure 2 that this turning point in the 3Q nutation profile holds for several rf frequencies and that the steepest slope is observed for smaller values of ω_1. Excitation of the 3Q coherence as a function of temperature may be used to detect changes in the quadrupole coupling constant that might be obscured by amorphous broadening or spectral overlap.

III. Experimental Section

NMR. Solid-state NMR spectra were acquired with custom designed spectrometers operating at 9.4 and 17.6 T. At 17.6 T, we used a custom designed transmission line probe with a Chemagnetics (Varian, Inc.)

(43) Goldman, M.; Grandinetti, P. J.; Llor, A.; Olejiniczak, Z.; Sachelleben, J. R.; Zwanziger, J. W. *J. Chem. Phys.* **1992**, *97*, 8947−8960.
(44) Maricq, M. M.; Waugh, J. S. *J. Chem. Phys.* **1979**, *70*, 3300−3316.
(45) Sun, B. Q.; Baltisberger, J. H.; Wu, Y.; Samoson, A.; Pines, A. *Solid State Nucl. Magn. Reson.* **1992**, *1*, 267−295.
(46) Hoult, D. I.; Richards, R. E. *J. Magn. Reson.* **1976**, *24*, 71−85.
(47) Wokaun, A.; Ernst, R. R. *J. Chem. Phys.* **1977**, *67*, 1752−1758.
(48) Vega, S. J. *J. Chem. Phys.* **1978**, *68*, 5518−5527.

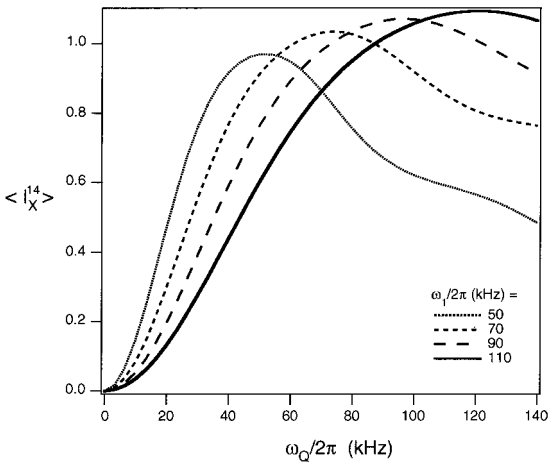

Figure 2. Calculation of 3Q excitation $\langle I_x^{14} \rangle$ as a function of the quadrupole coupling frequency, $\omega_Q = e^2qQ/h/2S(2S-1)$, and for various rf field strengths. These simulations were conducted in the GAMMA NMR simulation environment[54] which has been implemented in an in-house simulation package, QSI-v0.3. The secular terms of the 0th and 1st order quadrupole couplings are used in the Hamiltonian, along with 500 crystal orientations, 83 MHz Larmor frequency (corresponding to approximately 7.4 T for ^{23}Na), and 10-kHz MAS. The nutation pulse lengths used for each trace were 12 (50 kHz), 9 (70 kHz), 7 (90 kHz), and 5.5 μs (110 kHz).

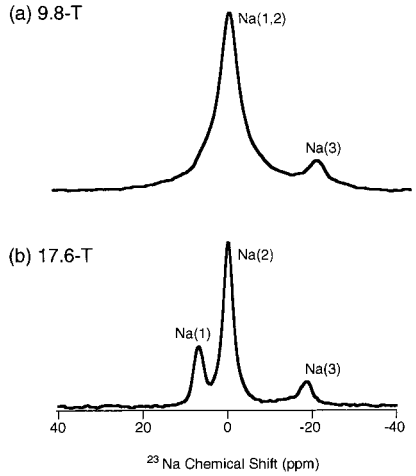

Figure 3. Magic-angle spinning ^{23}Na NMR spectra of d(TG_4T) at (a) 9.4 T from 1012 transients and 7 kHz MAS and (b) 17.6 T from 96 transients and 4.5 kHz MAS. Shifts are externally referenced to 0.1 M NaCl.

3.2 mm MAS housing, with moderate sample cooling (e.g., Figure 7) provided by precooling the spinning and bearing air sources. Sample temperature was stable to within ±1 °C.

Sample Preparation. The d(TG_4T) was chemically synthesized and purified as previously described for d($G_4T_4G_4$) (Smith & Feigon, 1993[49]). A 5 mM solution of the purified d(TG_4T) was dialyzed against 40 mM CsCl prior to drying in order to reduce the amount of Na^+ not coordinated within the quadruplex.[50] The final concentration of Na^+ in the solution sample was determined by comparing the integrated intensity of the ^{23}Na resonance (at 132.25 MHz) with the ^{23}Na resonance of a standard sample of 100 mM NaCl. This gave a final value for the solid sample of approximately three Na^+ per oligonucleotide strand. A critical concern in these experiments is to preserve the integrity of the sample during the drying steps for preparation of the sample for solid-state NMR studies. An additional problem sometimes encountered in solid-state NMR is the spectral broadening due to the amorphous nature of biological macromolecules in the solid phase. To address these concerns, we used a sample-packing approach which we term 'slow-drying'. It consisted of drying 20−30 μL aliquots of d(TG_4T) in the 3.2 mm rotor under anhydrous atmosphere ($P = 1$ atm) over a period of several hours. In combination with slow centrifugation (<1 G) of the entire rotor during drying, a small pellet forms at the bottom of the rotor. After the pellet is dry, the process is repeated until the rotor is full. This approach is intended to allow for proper folding and hydration. A comparison of ^{23}Na spectra of d(TG_4T) prepared via lyophilization and slow-drying (not shown) indicate that slow drying narrows the resonances by up to several hundred hertz and eliminates a broad amorphous signal. This broad baseline signal in the spectrum of lyophilized d(TG_4T) implies an amorphous character that may be due to the presence of unfolded or unstacked d(TG_4T) strands.

IV. Results

Magic-angle spinning (MAS) ^{23}Na spectra of d(TG_4T) at 9.4 T (105.22 MHz for ^{23}Na) and 17.6 T (198 MHz for ^{23}Na) are shown in Figure 3 where the high-field spectrum reveals three well-resolved sodium environments with good signal-to-noise. An exact comparison of sensitivity is complicated by hardware differences; however, it should be noted that the spectrum acquired at 9.4 T employed 10 times the number of transients as that acquired at 17.6 T, where lines are observed at 6.8, 0, and −19 ppm relative to 0.1 M NaCl solution. These are referred to as Na(1), Na(2), and Na(3), respectively, in the text and as marked in the figures.

The residual line widths for the MAS spectrum at 17.6 T are ≤1 kHz at half-maximum, and a potential source of line narrowing to be considered is motional averaging of the quadrupole coupling tensor. We investigated this with a series of variable-temperature ^{23}Na NMR spectra acquired with a dewared probe capable of MAS at temperatures ranging to −130 °C at 7.4 T. Although the lower static field limits resolution, this temperature series can indicate sample motions in several ways. First, if the quadrupole tensor becomes motionally constrained at lower temperatures, additional spectral broadening may be observed. This temperature series is shown in the left column of Figure 4 where a slight broadening of 100−200 Hz is measured and is somewhat visible when comparing the relative intensities of the Na(1,2) and Na(3) regions in the spectra at −80 °C and −120 °C. In this series of experiments, amorphous broadening and spectral overlap in the Na(1,2) region inhibit the observation of line broadening. An extension of this approach is to observe the effect of decoupling the proton spin bath through the temperature series since dipolar couplings will also be reintroduced as sample motions become constrained. The proton-decoupled spectra displayed in the middle column of Figure 4 illustrate that decoupling improves the signal-to-noise ratio below −40 °C.

Next, we introduce a new approach for detecting sample motions in the right column of Figure 4, where we measure the efficiency of 3Q coherence excitation for a single nutation pulse. The 3Q coherence generated by a nutation pulse is converted into central-transition coherence with a high-power, rotation-induced adiabatic coherence transfer (RIACT) pulse, which is less sensitive to the magnitude of the quadrupole coupling.[34] The dynamics of 3Q excitation were discussed in section II, where we identified conditions by which an increase in the excited 3Q coherence must correspond to an increase in the quadrupole coupling frequency. In the context of experiments performed over a temperature series, increasing 3Q excitation is interpreted as motional constraint of the quadrupole coupling tensor. We observe that appreciable 3Q coherence is barely detected in d(TG_4T) above −40 °C and conclude that the quadrupole coupling must be modulated by motion above this temperature.

(49) Smith, F. W.; Feigon, J. *Biochemistry* **1993**, *32*, 8682−8692.
(50) Deng, H.; Braunlin, W. H. *J. Mol. Biol.* **1996**, *255*, 476−483.

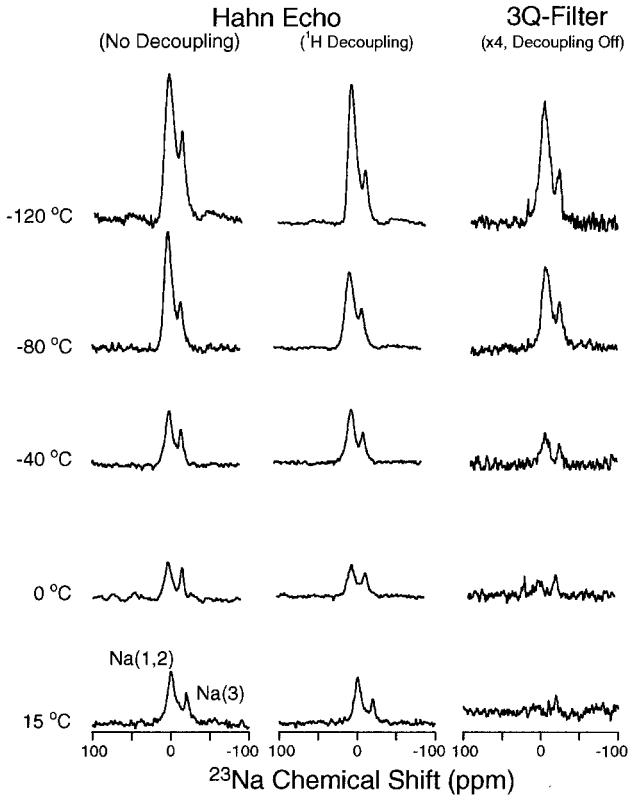

Figure 4. ^{23}Na MAS spectra of d(TG$_4$T) over a series of temperatures at 7.4 T (83 MHz for ^{23}Na) using (a) the Hahn-echo MAS experiment without proton decoupling, (b) the Hahn-echo experiment with proton decoupling, and (c) triple-quantum filtering without decoupling obtained by applying an RF nutation pulse with $\omega_1/2\pi = 50$ kHz for 3Q excitation followed by a high-power, $\omega_1/2\pi = 95$ kHz, RIACT pulse for reconversion into central transition coherence. Temperatures are indicated in the figure and were maintained to within ±0.5 °C; the sample was allowed to equilibrate for 20−25 min at each temperature before the experiments were acquired.

It is clearest from the right-hand column in Figure 4 that there are sample motions which can be quenched below −40 °C but which do not affect the observed line widths. This is understandable if we assume that the majority of the room-temperature line width is due to heterogeneous broadening resulting from the noncrystalline nature of the sample. Then the quadrupole coupling in the static limit must be too small to be observed with central transition spectroscopy. This is not surprising since the quadrupolar truncation at 17.6 T is quite substantial; for example, a moderate quadrupole coupling of $e^2qQ/h = 0.5$ MHz would give rise to a MAS line width of only ∼100 Hz (i.e., 0.5 ppm) at half-height.

To address the assignments for the three classes of sodium observed in Figure 3, we turned first to the MQMAS method[39] for recording isotropic spectra of half-integer quadrupolar nuclei. For the highest sensitivity, we performed the MQMAS experiment utilizing a nutation pulse for 3Q coherence excitation and a RIACT pulse for reconversion into the central transition.[34] The sheared, 2D-MQMAS spectrum at 9.4 T is shown in Figure 5, in which the signal at −19 ppm has a skewed 2D contour line shape which is not orthogonal to the $\omega_1/2\pi$ (high-resolution) axis. This effect has been discussed by Kentgens[28] and indicates a heterogeneous distribution of sites with similar quadrupole couplings but differing chemical shifts. The approximate shift position at −19 ppm is similar to the −13 ppm chemical shift observed for surface sodium ions in a lyophilized sample of

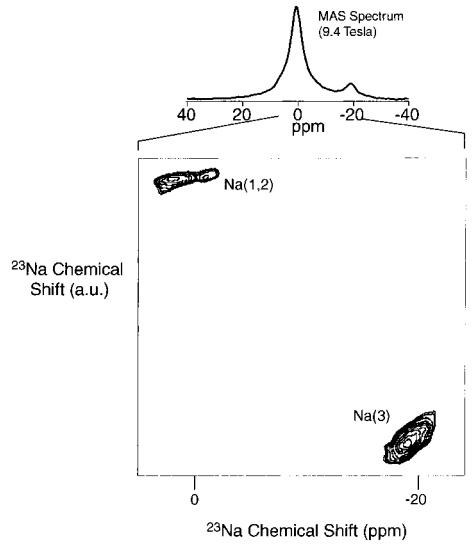

Figure 5. Sheared ^{23}Na multiple-quantum magic-angle spinning experiment at 9.4 T of d(TG$_4$T). A MAS spectrum is shown above. 64 t1 slices were acquired with 3000 transients per slice and a 1 s recycle delay. $\omega_1/2\pi = 170$ kHz.

calf-thymus DNA,[51] where an amorphous distribution of the sodium sites on and near the DNA surface was demonstrated. The difference in chemical shifts, −19 vs −13 ppm, is attributed to the difference in secondary structures. We therefore assign the Na(3) line in Figure 3 to sodium ions on the surface of the DNA. Although a signal is observed for the Na(1,2) region in Figure 4, the overlap at this field strength compromises interpretations other than the observation that the Na(1,2) region does not display the amorphous character of Na(3).

Multidimensional NMR spectroscopy is the canonical approach for obtaining assignments in spin-$^1/_2$ systems in liquid and solid samples.[24,25] However, there is a paucity of multidimensional methods for half-integer quadrupolar nuclei due to the complicated spin dynamics which result from the influence of the quadrupole coupling. Efforts to extend multidimensional methodology to quadrupolar nuclei include a recently described homonuclear correlation experiment among $S = {}^3/_2$ nuclei.[52] Here, we use the results of two complementary 2D experiments which corroborate the previous evidence and solve the remaining assignments.

First, the nutation behavior of the central-transition is exploited to determine the general magnitudes of the quadrupole couplings corresponding to the three signals observed in Figure 3 (section II). The amorphous broadening in Figure 3 clearly prevents any estimate of the quadrupole couplings so that an indirect method is required. We have recorded a 2D-MAS nutation spectrum by directly observing the ^{23}Na−NMR signal after an incrementable pulse (Figure 6a). Standard two-dimensional processing in magnitude mode should reveal the nutation frequencies of the lines in the spectrum, and this is shown in Figure 6b where it is clear that Na(1) and Na(3) are nutating in the regime $\omega_Q \gg \omega_1$, while Na(2) behaves in the limit of a vanishing quadrupole coupling (see eq 4). Noting also that Na(2) is observed at 0 ppm, it is straightforward to assign this line to free sodium salt. A similar nutation approach, but without the 2D processing, was used by He et al. in calf-thymus DNA studies.[51]

(51) He, H.; Klinowski, J.; Saba, G.; Casu, M.; Lai, A. *Solid State Nucl. Magn. Reson.* **1998**, *10*, 169−175.
(52) Baldus, M.; Rovnyak, D.; Griffin, R. G. *J. Chem. Phys.* **2000**, *112* (13), 5902−5909.

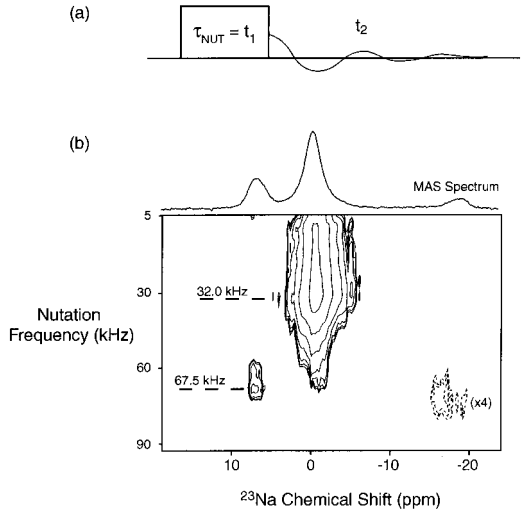

Figure 6. (a) Diagram of the pulse sequence for a 2D nutation experiment indicating the incremented single pulse, followed directly by acquisition. (b) 2D contour plot of the ^{23}Na nutation experiment obtained at 17.6 T in d(TG$_4$T) with 2D processing in magnitude mode. The nutation pulse was incremented in 2.5 μs steps up to 150 μs, with $\omega_r = 5.0$ kHz, and $T = 0$ °C. The Na(3) region was scaled by $\times 4$ to observe the nutation frequency of Na(3).

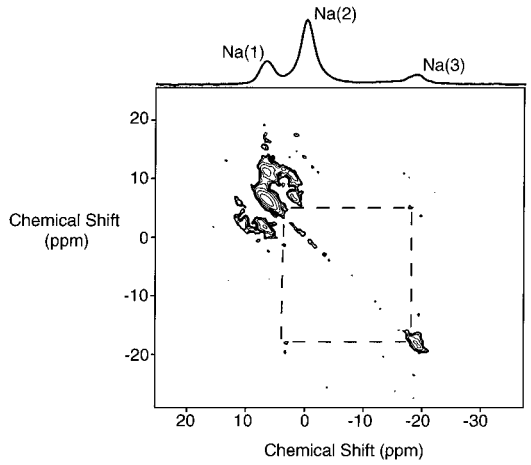

Figure 7. A 2D contour plot of an ^{23}Na-^{23}Na exchange (EXSY) experiment with mixing time $\tau_{mix} = 9$ ms, $\omega_r = 920$ Hz, and $T = -4.0$ °C. The temperature was controlled by cooling both the bearing and drive gas and monitored with a platinum thermistor placed next to the coil. An MAS spectrum is shown above to illustrate the spectral regions. All contours are positive.

Free and surface sodium sites are accounted for by the 2D MQMAS and nutation studies. Although it may be reasonable, in light of the unusual shift position (6.8 ppm), to conclude by elimination that Na(1) may be associated with channel sodium, this cannot be considered sufficient without more direct proof, which we obtained from analysis of a homonuclear correlation experiment. A ^{23}Na$-^{23}$Na correlation experiment was obtained by applying a standard three-pulse experiment in which chemical shift evolution is incremented after the first $\pi/2$ pulse, followed by a mixing period in which magnetization is stored along the longitudinal axis, and concluding with observation of chemical shift evolution again.[24] This is typically referred to as EXSY (exchange spectroscopy), and cross-peaks in the indirect dimension may arise due to true chemical exchange, direct dipolar cross-relaxation, or proton driven spin diffusion during the mixing period. The results of this experiment, for 8 ms mixing at -4 °C and with a 920 Hz MAS rate, are shown in Figure 7, where symmetric cross-peaks are clearly observed between Na(3) and the inside edge of Na(1). The observation of a coupling between Na(3) and Na(1) indicates that the surface sodium sites are proximate to a nonamorphous, chemically distinct class of sodiums which must reside on the interior. Reinforcing this is the fact that Na(1) nutates at twice the applied rf field strength, thus indicating a nonsymmetric, rigid environment. Thus Na(1) is conclusively associated with channel sodium sites.

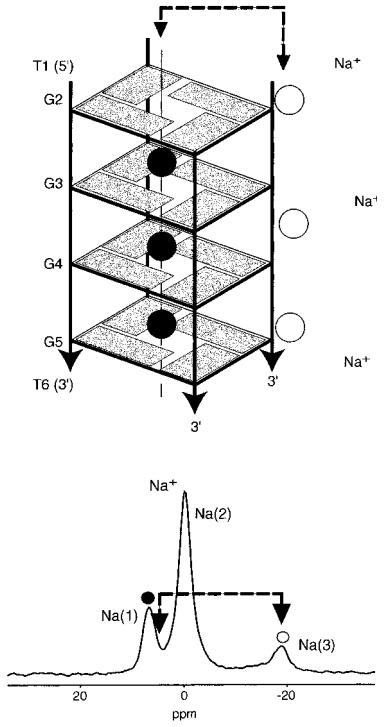

Figure 8. Diagram of the [d(TG$_4$T)]$_4$ quadruplex and the associated assignments of the free (Na$^+$), surface (open circles), and channel (filled circles) sodium signals to the high-field MAS spectrum shown below. The thymine bases at the 5′ and 3′ ends are not drawn in the figure and the numbering convention of Laughlan et al. is used.[42] The glycosyl bonds of the guanine bases (shaded rectangles) are all anti. The arrowed line on the spectrum and on the structure diagram indicates the homonuclear correlation between the surface (Na(3)) and channel (Na(1)) Na$^+$ ions, as shown in Figure 7.

V. Discussion

The assignments for channel, free, and surface sodium ions are graphically illustrated in Figure 8, in which the G-quartets are represented by the horizontal bars and the dashed arrow indicates the result of the homonuclear correlation experiment. As can be seen in Figure 1b, in the crystal structure of [d(TG$_4$T)]$_4$ the channel sodium ions are spaced at a distance slightly larger than that between quartets so that they are not located in identical local environments. In the two stacked quadruplexes, the first cation is in the plane of the quartet, while the most central ion is octahedrally coordinated by the carbonyls of two G-quartets and the rest are in distorted octahedral environments. We propose that this heterogeneity in local symmetry for the sodium ions observed in the crystal structure is also present in the solid sample and contributes to the broadening of Na(1). The existence of distinct resonances within the Na(1) line of Figure 3 is supported by the homonuclear correlation experiment (Figure 7), where the surface sodium correlates with the low-field edge of Na(1). This may indicate that proton-driven spin-diffusion is only occurring to the outermost channel sodium ions. It is not possible to determine

from these data whether the quadruplexes in the solid sample are stacked as in the crystal structure.

The ^{23}Na(3)−^{23}Na(1) homonuclear correlation could not be observed at higher MAS frequencies (2−6 kHz) and can be attributed to proton-driven spin diffusion. The cross-peaks are not perfectly symmetric; however, this is not unusual in solid-state 2D NMR. In particular, asymmetric cross-peak intensities may result when initial populations of the two exchanging species are not equal. The difficulty of applying true π and $\pi/2$ pulses to quadrupolar nuclei is well-known from the nutation behavior of the central transition in half-integer quadrupolar nuclei,[47,48] and so the asymmetry in the cross-peaks is attributed to inequivalent initial populations resulting from nutation effects.

The 3Q filtering approach introduced here (right-hand column, Figure 4) for gauging sample motions is in the same spirit as single-quantum static deuterium experiments.[53] In ^{2}H ($S = 1$) NMR of spin-labeled species, the quadrupole coupling and T_1 relaxation rates may be measured from static spectra acquired over a series of temperatures. The temperature dependence of the quadrupole coupling or ^{2}H relaxation may be compared to analytical models of the sample motions, often leading to the time scale and activation energy of the particular sample motions. Where ^{2}H studies fit the single-quantum line shape (or MAS sideband manifold) to extract quadrupole coupling parameters, the 3Q filter indicates the quadrupole coupling through the efficiency of 3Q excitation. The temperature series does not indicate that the sodium ions are undergoing exchange since there is no appearance of a narrow line corresponding to the fast exchange limit and the Na(1,2) and Na(3) regions are clearly resolved in the single quantum spectra at all temperatures. One possibility is that the motions are attributable to the d(TG_4T)$_4$ assemblies themselves. Isotropic reorientation or end-over-end rotation of the stacked assembly (Figure 1b) both incur obvious steric and energetic violations. In a solid or semisolid environment, axial rotation, similar to axial diffusion in phospholipids, is suggested to explain the motions in this sample. In principle, we could estimate the magnitude of the quadrupole coupling as a function of temperature and extract an approximate rate of axial diffusion. However such a procedure should first be extensively developed in model systems and this is beyond the scope of the present study. It is noted that the Na(1,2) region is more strongly influenced by the temperature series and that the data are not sufficient to confirm if axial diffusion represents the local motions in this sample.

(53) Vold, R.; Vold, R. L. *Deuterium Relaxation in Molecular Solids*. In *Advances in Magnetic and Optical Resonance*; Warren, W. S., Ed.; Academic Press: New York, 1991; p 85.

(54) Smith, S. A.; Levante, T. O.; Meier, B. H.; Ernst, R. R. *J. Magn. Reson. A* **1994**, *106*, 75.

Conclusion

The use of high fields is shown to be critical for studying half-integer quadrupolar nuclei in biological solids. Three classes of sodium are resolved for the d(TG_4T) DNA sample and sample motions were observed at temperatures as low as −40 °C. These motions are likely not attributable to any type of chemical exchange, but may be due to axial rotation of the stacked G-quartet assembly. A suite of 2D ^{23}Na NMR experiments were applied to assign the three classes of ^{23}Na to channel [(Na(1)], free [(Na(2)], and surface [Na(3)] environments at 6.8, 0, and −19 ppm, respectively. It is significant that resolution and assignments were achieved in a noncrystalline sample. The ability to resolve distinct cation environments and provide information on sample motions is complementary to X-ray studies and offers an additional benefit of not requiring sample crystallization. These experiments demonstrate the utility of solid-state NMR for studying cation binding to nucleic acids.

Acknowledgment. We are grateful to Dr. Chad Rienstra for the design of the 750 probe, to Dr. Jingui Hu for building the low-temperature 7.4-T MAS probe, and to Dr. Aneta Petkova for valuable discussions on conducting the variable-temperature experiments. M.B. acknowledges financial support of the Deutsche Forschungsgemeinschaft. This work was supported by NIH Grants GM48123 to J.F. and GM23403 and RR = 00 995 to R.G.G.

JA001022O